An immunogenic model of KRAS-mutant lung cancer enables evaluation of targeted therapy and immunotherapy combinations

Jesse Boumelha[1,17], Sophie de Carné Trécesson[1,17], Emily K. Law[9-12,17], Pablo Romero-Clavijo[1], Matthew A. Coelho[1,18], Kevin Ng[2], Edurne Mugarza[1], Christopher Moore[1], Sareena Rana[1,6], Deborah R. Caswell[4], Miguel Murillo[1,6], David C. Hancock[1], Prokopios P. Argyris[9-13], William L. Brown[9-11], Cameron Durfee[9-11,15], Lindsay K. Larson[9-11], Rachel I. Vogel[10,14], Alejandro Suárez-Bonnet[5,8], Simon L. Priestnall[5,8], Philip East[3], Sarah J. Ross[7], George Kassiotis[2], Miriam Molina-Arcas[1], Charles Swanton[4], Reuben Harris[9-12,15-16,19], Julian Downward[1,6,19]

[1] Oncogene Biology Laboratory, [2] Retroviral Immunology Laboratory [3] Bioinformatics and Biostatistics, [4] Translational Cancer Therapeutics Laboratory and [5] Experimental Histopathology,
Francis Crick Institute, 1 Midland Road, London NW1 1AT, UK
[6] Lung Cancer Group, Division of Molecular Pathology,
Institute of Cancer Research, 237 Fulham Road, London SW3 6JB, UK.
[7] AstraZeneca Oncology R&D, Cambridge CB4 0WG, UK
[8] Department of Pathobiology and Population Sciences, Royal Veterinary College, Hatfield, AL9 7TA, UK.
[9] Department of Biochemistry, Molecular Biology and Biophysics, University of Minnesota, Minneapolis, MN, USA, 55455
[10] Masonic Cancer Center, University of Minnesota, Minneapolis, MN, USA, 55455
[11] Institute for Molecular Virology, University of Minnesota, Minneapolis, MN, USA, 55455
[12] Howard Hughes Medical Institute, University of Minnesota, Minneapolis, MN, USA, 55455
[13] Division of Oral and Maxillofacial Pathology, School of Dentistry, University of Minnesota, Minneapolis, MN, USA, 55455
[14] Department of Obstetrics, Gynecology, and Women's Health, University of Minnesota, Minneapolis, MN, USA, 55455
[15] Department of Biochemistry and Structural Biology, University of Texas Health San Antonio, San Antonio, TX 78229, USA
[16] Howard Hughes Medical Institute, University of Texas Health San Antonio, San

Downloaded from http://aacrjournals.org/cancerres/article-pdf/doi/10.1158/0008-5472.CAN-22-0325/3186457/can-22-0325.pdf by University College of London user on 08 August 2022

Antonio, TX 78229, USA

[17] These authors contributed equally

[18] Present address: Sanger Institute, Hinxton CB10 1RQ, UK

[19] Correspondence:

Julian Downward, Francis Crick Institute, 1 Midland Road, London NW1 1AT, UK.

Telephone: +44(0)2037961838, email: julian.downward@crick.ac.uk

Reuben Harris, Department of Biochemistry and Structural Biology, University of Texas Health San Antonio, San Antonio, TX 78229, USA.

Telephone: +1 210 450 7300, email: rsh@uthscsa.edu

Conflict of interest statement: J.D. has acted as a consultant for AstraZeneca, Bayer, Jubilant, Theras, Vividion and Novartis. S.R. is an employee of AstraZeneca. C.S. receives grant support from Archer Dx, AstraZeneca, Boehringer–Ingelheim and Ono Pharmaceutical; has consulted for AstraZeneca, Bicycle Therapeutics, Celgene, Genentech, GRAIL, GSK, Illumina, Medicxi, MSD, Novartis and the Sarah Cannon Research Institute; receives grant support and has consulted for Bristol Myers Squibb, Pfizer and Roche–Ventana; is an advisory board member and is involved in trials sponsored by AstraZeneca; has stock options in Epic Sciences, GRAIL; and has stock options and is a co-founder of Achilles Therapeutics. The other authors declare that they have no potential conflicts of interest.

Downloaded from http://aacrjournals.org/cancerres/article-pdf/doi/10.1158/0008-5472.CAN-22-0325/3186457/can-22-0325.pdf by University College of London user on 08 August 2022

ABSTRACT

Mutations in oncogenes such as KRAS and EGFR cause a high proportion of lung cancers. Drugs targeting these proteins cause tumor regression but ultimately fail to elicit cures. As a result, there is an intense interest in how to best combine targeted therapies with other treatments, such as immunotherapies. However, preclinical systems for studying the interaction of lung tumors with the host immune system are inadequate, in part due to the low tumor mutational burden in genetically engineered mouse models. Here we set out to develop mouse models of mutant KRAS-driven lung cancer with an elevated tumor mutational burden by expressing the human DNA cytosine deaminase, APOBEC3B, to mimic the mutational signature seen in human lung cancer. This failed to substantially increase clonal tumor mutational burden and autochthonous tumors remained refractory to immunotherapy. However, establishing clonal cell lines from these tumors enabled the generation of an immunogenic syngeneic transplantation model of KRAS-mutant lung adenocarcinoma that was sensitive to immunotherapy. Unexpectedly, anti-tumor immune responses were not directed against neoantigens but instead targeted derepressed endogenous retroviral antigens. The ability of KRASG12C inhibitors to cause regression of KRASG12C-expressing tumors was markedly potentiated by the adaptive immune system, highlighting the importance of using immunocompetent models for evaluating targeted therapies. Overall, this model provides a unique opportunity for the study of combinations of targeted and immunotherapies in immune-hot lung cancer.

STATEMENT OF SIGNIFICANCE

This study develops a mouse model of immunogenic KRAS-mutant lung cancer to facilitate the investigation of optimal combinations of targeted therapies with immunotherapies.

Downloaded from http://aacrjournals.org/cancerres/article-pdf/doi/10.1158/0008-5472.CAN-22-0325/3186457/can-22-0325.pdf by University College of London user on 08 August 2022

INTRODUCTION

Non-small cell lung cancer (NSCLC) is the leading cause of cancer-related deaths worldwide (1). With less than 20% of NSCLC patients surviving more than 5 years (2), there is a pressing need for novel therapeutic strategies. Oncogenic mutations in KRAS, a member of the RAS family of small GTPases, occur in 20-30% of patients with NSCLC (3) and drive multiple processes that promote tumour development. Despite much effort, targeted therapies that directly inhibit signalling pathways downstream of KRAS have shown limited success in the clinic for NSCLC patients (4). However, the recent emergence of immune checkpoint blockade (primarily anti-PD(L)-1 agents), which can reverse tumour-driven immune suppression and unleash powerful anti-tumour immune responses, has transformed the treatment of NSCLC, achieving durable responses in some patients (5). Unfortunately, as seen in other tumour types, only a subset of patients responds to immune checkpoint blockade (ICB).

It has therefore become critical to further elucidate the molecular determinants that underpin the interaction between the tumour and the immune system. Increasing evidence suggests that tumour-cell-intrinsic oncogenic signalling, including KRAS signalling (6), can hamper anti-tumour immune responses and there is considerable interest in using targeted therapies to broaden the clinical response to ICB. The recent development of $KRAS^{G12C}$ inhibitors, which target the most common mutant form of the protein in lung cancer, has shown that inhibiting KRAS-signalling in tumour cells promotes anti-tumour immune responses and synergises with anti-PD-1 therapy in an immune-competent model of colorectal cancer (7).

Identifying rational therapeutic approaches to extend the clinical benefits of current ICBs in NSCLC requires preclinical models that recapitulate the interactions between tumour cells and the immune system, which is not possible in conventional xenograft models lacking a functional immune system. Genetically engineered mouse models (GEMMs) have been extensively used to gain mechanistic insights into the biology of KRAS-mutant lung cancer and to assess the efficacy of novel therapeutics. Such models recapitulate key aspects of the human disease in an immune-competent setting, however, they fail to elicit strong anti-tumour immune responses (8,9) and therefore have limited use for studying tumour-immune interactions. Genetically engineered mouse cancer models usually feature a small number of introduced strong

Downloaded from http://aacrjournals.org/cancerres/article-pdf/doi/10.1158/0008-5472.CAN-22-0325/3186457/can-22-0325.pdf by University College of London user on 08 August 2022

driver mutations, sufficient for tumorigenesis, and acquire few additional mutations. Tumours arising from these models therefore have a low tumour mutational burden (TMB) compared to their human counterparts (10), limiting the presentation of neoantigens to the adaptive immune system. This problem has been overcome by the forced expression of highly immunogenic antigens, such as ovalbumin (9,11), but it is unclear whether the strong anti-tumour immune responses elicited by such foreign antigens reflect those in human cancers which occur towards less potent neoantigens and tumour-associated antigens.

To address this issue, we set out to generate a novel mouse model of KRAS driven lung adenocarcinoma with increased tumour mutation burden and increased immunogenicity. Approaches used included the use of carcinogens and also the over-expression of a member of the APOBEC family of single-stranded DNA deaminases, which are responsible for inducing mutations in a range of cancers (12). We were ultimately successful in generating a transplantable KRAS mutant lung cancer model that is partially sensitive to immunotherapy and shows a response to KRAS targeted agents that is potentiated by adaptive immunity. This transplantable lung cancer model will be a valuable tool for studying strategies for combining targeted agents against the RAS pathway with immunotherapies.

Downloaded from http://aacrjournals.org/cancerres/article-pdf/doi/10.1158/0008-5472.CAN-22-0325/3186457/can-22-0325.pdf by University College of London user on 08 August 2022

MATERIALS AND METHODS

In vivo tumour studies

All studies were performed under an animal research ethics project license that was approved by the UK Home Office and in accordance with institutional welfare guidelines.

Kras$^{LSL\text{-}G12D/+}$;*Trp53*$^{fl/fl}$ mice (KP) were sourced from the Mouse Models of Human Cancer Consortium and maintained on a pure C57BL/6 background. *Kras*$^{LSL\text{-}G12D/+}$; *Trp53*$^{fl/fl}$;*Rosa26*^{A3Bi} mice (KPA) and *Kras*$^{LSL\text{-}G12D/+}$*Trp53*$^{fl/fl}$;*Rosa26*^{A3Bi};*Rag1*$^{-/-}$ mice (KPAR) were generated by breeding KP mice with *Rosa26*^{A3Bi} mice and *Rag1*$^{-/-}$ mice (see Supplementary Methods for development and validation of the *Rosa26::LSL-A3Bi* model). Tumours were induced by intratracheal intubation of 1x10^6 adenovirus expressing Cre recombinase as previously described (13). Tumour volume was assessed via micro-CT scanning.

For the urethane-induced models, tumours were induced by 3 intra-peritoneal injections of 1mg/g of urethane over the period of a week. Three weeks following urethane first injection, APOBEC3Bi was induced by 3 doses of 100mg/g tamoxifen over a period of a week in *Rosa26*$^{A3Bi/CreER(t2)}$ mice (UrA3Bi-CreER). Tumour volume was assessed via micro-CT scanning.

All transplantation animal experiments were carried out using 8-12-week C57BL/6 mice. For subcutaneous studies, 1.5x10^5 KPAR1.3 or KPAR1.3^{G12C} cells and 5x10^5 KPB6^{G12C} cells (1:1 mix with Matrigel) were injected subcutaneously into the flank. Tumour volume was measured twice weekly and calculated using the formula 0.5 x [Length x Width^2]. Mice were euthanised when the average tumour dimensions exceeded 1.5 mm. For re-challenge experiments, tumour-free mice were injected subcutaneously into the opposite flank with 1.5x10^5 KPAR1.3 tumour cells. For orthotopic studies, 1.5x10^5 KPAR1.3 cells, 1x10^5 KPAR1.3^{G12C} and KPB6 cells were injected intravenously into the tail-vein. Mice were euthanised when the humane endpoint of 15% weight loss was reached.

For treatments, 200µg anti-PD-1 (clone RMP1-14, BioXcell) and 200µg anti-CTLA-4 (clone 9H10, BioXcell), or their respective IgG controls, were administered per mouse via intraperitoneal injection twice weekly for a maximum of three weeks. Anti-PD-L1 (clone 10F.9G2, BioXcell) or the respective IgG control were administered at 10 mg/kg via intraperitoneal injection twice weekly, for two weeks. AZ-8037 or vehicle

Downloaded from http://aacrjournals.org/cancerres/article-pdf/doi/10.1158/0008-5472.CAN-22-0325/3186457/can-22-0325.pdf by University College of London user on 08 August 2022

(10% Pluronic-F127) was administered 5 days per week via oral gavage at 100mg/kg. Mice were randomised into groups and treatments initiated once tumours reached an average volume of 150mm^3 for subcutaneous studies or were detectable by micro-CT for orthotopic experiments.

Cell lines

The KPB6 cell line was obtained from Cell Services at the Francis Crick Institute. KPAR and KPA cell lines were established by cutting up lung tumours into small pieces and culturing in DMEM-F12 supplemented with Glutamax®, FBS (10%), hydrocortisone (1μM), EGF (20ng/ml), IGF (50ng/ml), penicillin (100units/mL) and streptomycin (100μg/mL). Clonal cells were derived by single-cell dilution into 96 well plates. *Emv2*$^{-/-}$ KPAR cells were generated by CRISPR/Cas9-mediated genetic deletion. Cell lines were routinely tested for *Mycoplasma*.

Flow cytometry

Mouse tumours were cut into small pieces, incubated with collagenase (1mg/ml; ThermoFisher) and DNase I (50U/ml; Life Technologies) for 45 min at 37°C and filtered through 70μm strainers (Falcon). Red blood cells were lysed for 5 min using ACK buffer (Life Technologies). Cells were stained with fixable viability dye eFluor870 (BD Horizon) for 30 min and blocked with CD16/32 antibody (Biolegend) for 10 min. Cells were then stained with one of three antibody cocktails for 30 min (see Supplementary Table 2). Intracellular staining was performed using the Fixation/Permeabilization kit (eBioscience) according to the manufacturer's instructions. Samples were analysed using a BD Symphony flow cytometer. Data was analysed using FlowJo (Tree Star).
For FACS analysis *in vitro*, cells were trypsinised, washed with FACS buffer and stained for eMLV envelope glycoprotein using the 83A25 monoclonal antibody followed by a secondary staining with anti-rat IgG2a. Samples were run on LSRFortessa (BD).

Histopathology and Immunohistochemistry

Tumour-bearing lungs were fixed in 10% NBF for 24h followed by 70% ethanol. Fixed tissue was embedded in paraffin wax. Tissue sections were stained with haematoxylin and eosin, using standard methods. Sections were examined by two board-certified veterinary pathologists (ASB and SLP).

Downloaded from http://aacrjournals.org/cancerres/article-pdf/doi/10.1158/0008-5472.CAN-22-0325/3186457/can-22-0325.pdf by University College of London user on 08 August 2022

For immunohistochemistry staining, tissue sections were boiled in sodium citrate buffer (pH 6.0) for 15min and incubated with the following antibodies for 1h: anti-Foxp3 (D6O8R, CST), anti-CD8 (4SM15, Thermo Scientific) and anti-A3B (5210-87-13) (14). Primary antibodies were detected using biotinylated secondary antibodies and detected by HRP/DAB. Slides were imaged using a Leica Zeiss AxioScan.Z1 slide scanner.

Micro-CT imaging

Mice were anesthetised by inhalation of isoflurane and scanned using the Quantum GX2 micro-CT imaging system (Perkin Elmer). Serial lung images were reconstructed and tumour volumes subsequently analysed using Analyse (AnalyzeDirect).

Exome sequencing and neoantigen prediction

Genomic DNA was extracted from tumours, cell lines and mouse tails using DNeasy Blood & Tissue kit (Qiagen). Exome libraries were prepared by the Advanced Sequencing Facility at the Crick and sequenced using an Illumina HiSeq 4000 using 100 base pair paired-end reads. Reads were aligned to the GRCm38 mouse genome and tumour specific somatic mutations called against matched tail samples from the same animal using Mutect1 (v1.1.7) and Mutect2 (GATK v4.1.3.0). For details, see Supplementary Methods. Mutated peptide sequences were processed using NetMHC4.0 with *k*-mer of 8-11 length. Rank threshold of 0.5, or 2.0, were used to identify putative strong, or weak, MHC-I (H2-Kb and H2-Db) binders, respectively.

qPCR

Total RNA was extracted from cell lines or frozen tumour samples using RNeasy kit (Qiagen). Frozen tumour samples were homogenised prior to RNA extraction either using a syringe and needle or QIAshredder columns (Qiagen). cDNA was synthesised using Maxima First Strand cDNA Synthesis Kit (ThermoFisher) and qPCR was performed using Fast SYBR™ Green Master Mix (ThermoFisher). mRNA relative quantity was calculated as previously described (15) and normalised to at least three housekeeping genes. See Supplementary Table 3 for list of qPCR primers.

Downloaded from http://aacrjournals.org/cancerres/article-pdf/doi/10.1158/0008-5472.CAN-22-0325/3186457/can-22-0325.pdf by University College of London user on 08 August 2022

Tumour Cell Viability

For short-term viability assays, $1.5x10^3$ KPAR1.3^{G12C} or $2x10^3$ KPB6^{G12C} cells were seeded in 96-well plates and grown in the presence of different inhibitors for 72h. Cell viability was assessed using CellTiter-Blue (Promega).

Western blotting

Cells were lysed using protein lysis buffer (Sigma) with protease and phosphatase inhibitor cocktails (Sigma). Protein concentration was determined using a BCA protein assay kit (Pierce). 15-20µg of protein was separated on a 4-12% Bis-Tris gel (Life Technologies) and transferred to PVDF membranes. Protein expression was detected by Western blotting using the following primary antibodies against: S6 (54D2, Cell Signalling), p-S6 (Ser235/236) (2211, Cell Signalling), Erk1/2 (3A7, Cell Signalling), p-Erk1/2 (Thr202/Tyr204) (9101, Cell Signalling), Akt (40D4, Cell Signalling), p-Akt (Ser473) (D9E, Cell Signalling), and Vinculin (VIN-11-5, Sigma). Primary antibodies were detected with HRP-conjugated anti-rabbit or anti-mouse IgG and visualised with Immobilon Western HRP substrate (Merck).

ELISA

CXCL9 and CXCL10 were quantified from 300µg of tumour protein lysates using Duoset ELISA kits (R&D) according to the manufacturer's instructions.

ELISpot analysis

Either $1x10^5$ splenocytes or $1x10^4$ CD8$^+$ TILs, isolated from tumours using the EasySep Mouse CD8α Positive Selection Kit (Stemcell Technologies), were harvested from tumour-bearing mice and pulsed with 1µM peptide corresponding to clonal neoantigens predicted from KPAR1.3 WES (Supplementary Table 1) or eMLV *env* peptide (KSPWFTTL). TILs were co-incubated with $1x10^5$ splenocytes from naïve mice as a source of dendritic cells. Cells were stimulated for 24h in anti-mouse IFNγ-coated ELISpot plates (BD Bioscience). Plates were developed according to manufacturer's instructions and quantified using a CTL S6 machine.

Data Availability

The sequencing data for this study have been deposited in the European Nucleotide Archive (ENA) at EMBL-EBI under accession number PRJEB53982

Downloaded from http://aacrjournals.org/cancerres/article-pdf/doi/10.1158/0008-5472.CAN-22-0325/3186457/can-22-0325.pdf by University College of London user on 08 August 2022

(https://www.ebi.ac.uk/ ena /browser/ view/PRJEB53982). All other data is included in the paper and supplement.

Downloaded from http://aacrjournals.org/cancerres/article-pdf/doi/10.1158/0008-5472.CAN-22-0325/3186457/can-22-0325.pdf by University College of London user on 08 August 2022

RESULTS

Autochthonous KP lung tumours do not engage with the adaptive immune system

The introduction of adenovirus expressing Cre recombinase (AdCre) into the lungs of *Kras*$^{LSL\text{-}G12D/+}$;*Trp53*$^{fl/fl}$ (KP) mice leads to expression of oncogenic Kras^{G12D} and deletion of p53 in lung epithelial cells, resulting in the induction of lung adenocarcinoma (16). This system represents one of the most widely used mouse models of lung cancer. To assess the immunogenicity of lung tumours in KP mice, we crossed them onto a *Rag2*$^{-/-}$ background, which lacks mature T and B cells, and monitored tumour growth by micro-computed tomography (micro-CT) imaging. Adaptive immunity was unable to constrain the growth of KP tumours as they grew at similar rates in immune-competent (*Rag2*$^{+/-}$) and immune-deficient (*Rag2*$^{-/-}$) mice (Fig. 1A, B). To assess whether an adaptive immune response could be generated against KP tumours, we treated tumour-bearing mice with a combination of anti-PD-L1 and anti-CTLA-4 (Fig. 1C). This combination therapy failed to delay tumour growth (Fig. 1D, E) and did not lead to an increase in the survival of tumour-bearing mice (Fig. 1F). It has previously been shown that MEK inhibition enhances anti-tumour immunity and synergises with anti-PD-L1 in KRAS-mutant CT26 colorectal tumours (17). However, we found that the combination of anti-PD-L1 and trametinib failed to control KP tumour growth compared to trametinib alone (Supplementary Fig. 1A-C). These data suggest that the adaptive immune system cannot recognise autochthonous KP tumours.

Human APOBEC3B does not induce immunogenicity in KP or carcinogen-induced lung tumours

Compared to human lung cancer, KP mouse lung tumours exhibit very few mutations necessary to generate neoantigens that can make tumour cells visible to the immune system (10). APOBEC3B is a single-stranded DNA cytosine deaminase that induces C>T/G substitutions in several solid cancers (12,18). APOBEC3B expression increases during NSCLC progression(19) and has been associated with intra-tumoral heterogeneity (20,21). Analysis of lung adenocarcinoma (LUAD) samples from The Cancer Genome Atlas (TCGA) revealed that the mutational rate of non-synonymous APOBEC mutations was lower in comparison with other types of

Downloaded from http://aacrjournals.org/cancerres/article-pdf/doi/10.1158/0008-5472.CAN-22-0325/3186457/can-22-0325.pdf by University College of London user on 08 August 2022

mutation, suggesting that non-synonymous mutations generated by APOBEC could be immunogenic and preferentially eliminated by the immune system (Fig. 2A).

We therefore decided to express human APOBEC3B in the KP model to increase the frequency of mutations in these tumours to promote the generation of neoantigens that could stimulate adaptive anti-tumour immune responses. We inserted a human *APOBEC3B* minigene (*A3Bi*) in the *Rosa26* locus under the control of a lox-STOP-lox cassette so that its expression is inducible upon exposure of cells to Cre recombinase (Supplementary Fig. 2A-J). A3Bi expression alone did not induce tumours and did not decrease the lifespan of the mice (Supplementary Fig. 2K-L). We crossed the mice with KP mice to generate *Kras*$^{G12D/+}$;*Trp53*$^{fl/fl}$;*Rosa26*^{A3Bi} (KPA) mice. Following intratracheal AdCre delivery, A3Bi is initially expressed in the same cells as those that undergo *Kras*^{G12D} expression and *Trp53* deletion (Supplementary Fig. 3A). As expected, we observed A3Bi protein expression in the nucleus of the tumour cells, however, tumours contained different percentages of A3Bi-expressing cells (Fig. 2B and Supplementary Fig. 3B) as well as heterogeneous levels of expression (Fig. 2C), suggesting a selection pressure against A3Bi expression during tumour growth. Consistent with this, KPA tumours were of lower grade compared to KP tumours, had a lower percentage of mitotic cells and showed a moderate CD8$^+$ T cell infiltration – although most CD8$^+$ T cells accumulated at the periphery of the tumours (Fig. 2D-G and supplementary Fig. 3C). However, KPA tumours grew at similar rates to KP tumours (Supplementary Fig. 3D), suggesting other mechanisms triggered by APOBEC3B expression could affect tumour growth.

To address this issue and assess whether the increased CD8$^+$ T cell recruitment in KPA tumours promoted immune control, we crossed KPA mice onto a *Rag1*$^{-/-}$ background (KPAR) and evaluated tumour growth in KPA and KPAR animals. We observed no differences in tumour number, growth, or survival in KPAR mice compared with KPA mice (Supplementary Fig. 3E-G). We also treated KP and KPA tumour-bearing mice with anti-PD-1 and anti-CTLA-4 and observed no differences between the two groups (Fig. 2H and Supplementary Fig. 3H). We then performed whole-exome sequencing (WES) of KP and KPA tumours to assess whether A3Bi expression increased tumour mutational burden and neoantigens. We found that the total number of subclonal exonic SNVs and predicted neoantigens were moderately increased in A3Bi-expressing tumours (Fig. 2I-J). However, the majority of these were

Downloaded from http://aacrjournals.org/cancerres/article-pdf/doi/10.1158/0008-5472.CAN-22-0325/3186457/can-22-0325.pdf by University College of London user on 08 August 2022

not typical A3Bi T(C>T/G) mutations, suggesting indirect mechanisms linking APOBEC3B with the formation of new mutations (Supplementary Fig. 3I-J).

Altogether, these findings suggest that A3Bi expression in the KP model of lung adenocarcinoma did not produce sufficient immunogenic mutations to elicit an adaptive immune response. This may be partly because of the heterogeneity of A3Bi expression in the tumours, the subclonal nature of any potential neoantigens, or due to insufficient numbers of mutations induced in this system.

Murine KP tumours develop extremely rapidly, inducing a life-threatening tumour burden in about 14 to 18 weeks. We reasoned that the aggressive nature of the KP model did not allow sufficient time for APOBEC3B to induce mutations during tumour development, leading to only a few detectable SNVs with low allelic frequency. Carcinogen-induced tumours tend to be less aggressive than GEMMs and develop more slowly. To extend the length of tumour development, we exposed the mice to urethane before A3Bi expression. Urethane is a carcinogen which induces A>T/G substitutions and initiates lung tumours by inducing an activating mutation at codon Q61 in *Kras* (22,23). To model A3Bi expression in carcinogen-induced tumours we initiated tumours with urethane in *Rosa26*$^{A3Bi/CreER(t2)}$ mice (UrA3Bi) which when treated with tamoxifen express A3Bi in all tissues. Since APOBEC mutations are often late events in tumour evolution (20), we delayed the induction of A3Bi by three weeks after the first injection of urethane (Supplementary Fig. 4A).

Consistent with our observation in the KPA model, A3Bi expression was downregulated in tumours compared with adjacent lung (Fig. 2K), suggesting a selective pressure against A3Bi expression in tumours. Tumour growth and the number of tumours per animal were also similar between urethane and UrA3Bi tumours (Supplementary Fig. 4B-C). In contrast, UrA3Bi tumours had more advanced histological grades than tumours induced by urethane alone (Fig. 2L).

Interestingly, flow cytometry analysis revealed increased activation of tumour-infiltrating CD8$^+$ T cells in UrA3Bi tumours with increased expression of the early activation marker CD69 and the immune checkpoint receptor LAG-3 (Supplementary Fig. 4D). However, as with the KPA model, co-treatment with anti-PD-1 and anti-CTLA-4 failed to control tumour growth (Fig. 2M). We performed WES to assess the mutation burden in UrA3Bi tumours. As expected, urethane exposure generated a substantial number of clonal exonic SNVs (Fig. 2N and Supplementary Fig. 4E). In all UrA3Bi tumours but one, we observed an increase in total SNVs and neoantigens (Fig.

Downloaded from http://aacrjournals.org/cancerres/article-pdf/doi/10.1158/0008-5472.CAN-22-0325/3186457/can-22-0325.pdf by University College of London user on 08 August 2022

2N-O and Supplementary Fig. 4E-F). Unfortunately, the small number of samples in this study did not provide sufficient statistical power to determine if this difference was significant. Like in the KPA model, A3Bi expression failed to induce typical APOBEC T(C>T/G) mutations (Supplementary Fig. 4E) and predicted neoantigens (Supplementary Fig. 4F).

To summarise, as with the KP model, APOBEC3B expression failed to induce immunogenicity in carcinogen-induced models of lung cancer.

Establishment of immunogenic clonal cell lines from KPAR tumours

We hypothesised that the lack of immunogenicity in APOBEC3B-expressing autochthonous tumours might be due to the subclonality of mutations, which have been shown to be less effective at generating effective adaptive immune responses (24,25). We therefore established cell lines from these models which were subsequently single-cell cloned to increase the frequency of clonal neoantigens. Cell lines established from urethane-induced tumours grew poorly *in vitro* and failed to grow when transplanted into mice, probably as urethane-induced tumours are typically very low grade and often only possess a mutation in Kras (Q61R), lacking any further oncogenic alterations. However, a number of cell lines were readily established from KPA and KPAR autochthonous tumours and single-cell cloned. We were unable to detect APOBEC3B mRNA expression in any of the KPAR cell lines (Fig. 3A), suggesting that expression of the transgene was downregulated during tumour growth, consistent with what we observed by immunohistochemistry (Fig. 2B). In contrast, APOBEC3B mRNA expression was detected in the KPA cell lines and therefore we decided not to further characterise them as the expression of a human recombinant protein could affect the growth of transplanted tumours in immune-competent hosts.

The immunogenicity of different single-cell KPAR clones was assessed by comparing the growth of cells subcutaneously transplanted into syngeneic immune-competent and immune-deficient (*Rag1*$^{-/-}$) mice. KPAR1.1 cells grew similarly when injected into immune-competent and *Rag1*$^{-/-}$ mice whilst two other clones, KPAR1.3 and KPAR1.5, grew more slowly in immune-competent mice compared to *Rag1*$^{-/-}$ mice (Fig. 3B and Supplementary Fig. 5A).

We carried out WES to assess the mutational burden of the KPAR clonal cell lines, the parental polyclonal cell line (KPAR1) and another autochthonous KPAR tumour

Downloaded from http://aacrjournals.org/cancerres/article-pdf/doi/10.1158/0008-5472.CAN-22-0325/3186457/can-22-0325.pdf by University College of London user on 08 August 2022

taken from the same mouse. Single-cell cloning moderately increased the frequency of detectable mutations (Fig. 3C). All single-cell clones contained more mutations compared with the parental cell line or KP tumours (Fig. 2I). However, the number of mutations in all clonal cell lines was still very low compared to other transplantable syngeneic cancer cell lines, and immunogenic KPAR1.3 cells did not possess more predicted neoantigens than non-immunogenic KPAR1.1 cells (Fig. 3D, Supplementary Table S1). Notably, very few mutations were typical APOBEC T(C>T/G) mutations (Supplementary Fig. 5B). Furthermore, we were unable to detect antigen-specific $CD8^+$ T cells against predicted clonal neoantigens when pulsing splenocytes isolated from KPAR1.3 tumour-bearing mice in an IFNγ enzyme-linked immune absorbent spot (ELISpot) assay (Fig. 3E, Supplementary Table S1).

Given that A3Bi failed to directly induce any immunogenic mutations in the KPAR1.3 cell line we asked whether the immunogenicity of this cell line may be due to another source of antigens. One major class of tumour-associated antigens consists of endogenous retroviral proteins that are often derepressed in established mouse cancer cell lines (26) and have also been shown to drive anti-tumour immune responses in human cancer (27). Interestingly, ELISpot analysis revealed that the major MHC-I restricted epitope arising from the envelope glycoprotein (*env*) of *Emv2*, the endogenous ecotropic murine leukaemia retrovirus (eMLV) in C57BL/6J mice, induced IFNγ secretion from splenocytes harvested from KPAR1.3 tumour-bearing mice (Fig. 3E). Consistent with this, immunogenic KPAR1.3 and KPAR1.5 clones expressed significantly higher levels of the eMLV envelope glycoprotein compared to the non-immunogenic KPAR1.1 cell line (Supplementary Fig. 5C). To assess whether eMLV derived antigens contributed to the immunogenicity of KPAR1.3 tumours we generated *Emv2*$^{-/-}$ KPAR1.3 cells using CRISPR-Cas9. Genetic deletion of the *Emv2* locus was confirmed by loss of eMLV envelope expression (Supplementary Fig. 5D). *Emv2*$^{-/-}$ KPAR1.3 cells grew at similar rates to parental KPAR1.3 cells after subcutaneous transplantation into *Rag1*$^{-/-}$ mice but grew significantly faster in immune-competent mice (Supplementary Fig. 5E).

Together these results indicate that the immunogenicity of the KPAR1.3 cell line was not due to tumour mutational burden, but elevated expression of endogenous retroviral antigens that stimulate endogenous $CD8^+$ T cell responses.

Downloaded from http://aacrjournals.org/cancerres/article-pdf/doi/10.1158/0008-5472.CAN-22-0325/3186457/can-22-0325.pdf by University College of London user on 08 August 2022

KPAR tumours generate an adaptive immune response

Although immunogenicity of the KPAR1.3 cell line was not due to neoantigens generated by non-synonymous mutations as we initially hypothesised, the novelty of an immunogenic transplantable murine lung cancer cell line warranted further characterisation. We therefore used flow cytometry to characterise the tumour microenvironment of orthotopic lung tumours established from immunogenic KPAR1.3 cells (from now on referred to as KPAR) and non-immunogenic KPB6 cells, derived from the original KP GEMM on a C57BL/6 background. Notably, KP tumours have very few predicted neoantigens (Fig. 2I) and KPB6 cells display significantly reduced surface expression of the eMLV envelope protein compared to KPAR cells (Supplementary Fig. 5F).

The immune compartment of both tumour models differed significantly compared to normal lung with a large increase in the proportion of myeloid cells, consisting primarily of interstitial macrophages, and exclusion of B cells and NK cells (Fig. 4A, Supplementary Fig. 6). KPB6 tumours contained significantly more myeloid cells than KPAR tumours, primarily due to an increased proportion of neutrophils (Supplementary Fig. 7A). Conversely, KPAR tumours showed significantly higher levels of T cell infiltration, which was a result of increased $CD8^+$ and $CD4^+$ T cells and regulatory T (Treg) cells, as well as increased NK cell infiltration (Fig. 4B). Immunohistochemistry staining confirmed that KPAR tumours were more infiltrated with $CD8^+$ T cells (Supplementary Fig. 7B). T cells infiltrating KPAR tumours were also more activated, with a higher proportion of effector memory $CD8^+$ and $CD4^+$ T cells (Fig. 4C) and increased expression of the activation marker CD44 on both $CD8^+$ and $CD4^+$ T cells (Supplementary Fig. 7C-D) as well as the early activation marker CD69 on $CD8^+$ T cells (Supplementary Fig. 7E). Both $CD8^+$ and $CD4^+$ T cells also showed increased expression of the immune checkpoint molecules PD-1, LAG-3 and TIM-3 in KPAR tumours (Fig. 4D). Furthermore, KPAR tumours also contained a significant proportion of PD-1/LAG-3 double-positive $CD8^+$ T cells which were completely absent in KPB6 tumours (Fig. 4E). There was also an increased proportion of PD-$L1^+$ myeloid cells in KPAR tumours, indicative of a T-cell inflamed tumour microenvironment (Fig. 4F).

Taken together, these data demonstrate that orthotopic KPAR tumours generated an adaptive anti-tumour immune response which was absent in orthotopic KPB6 tumours.

Downloaded from http://aacrjournals.org/cancerres/article-pdf/doi/10.1158/0008-5472.CAN-22-0325/3186457/can-22-0325.pdf by University College of London user on 08 August 2022

KPAR tumours are responsive to ICB

Given that the growth of KPAR tumours was partially restrained by adaptive immunity and orthotopic tumours were highly infiltrated with activated immune cells, we next tested the sensitivity of the model to ICB. Mice bearing subcutaneous KPAR tumours were treated with anti-PD-1, anti-CTLA-4 or a combination of both. Anti-CTLA-4 alone, or in combination with anti-PD-1, led to tumour regression in all mice, whilst anti-PD-1 alone failed to affect tumour growth (Fig. 5A, and Supplementary Fig. 8A). Furthermore, anti-CTLA-4 or the combination of anti-CTLA-4 and anti-PD-1 resulted in long-term durable regression for up to one year in 33% and 50% of mice, respectively (Fig. 5B). All treated mice that had rejected the primary tumour subsequently rejected a secondary tumour when re-challenged with KPAR cells on the opposite flank (Fig. 5B), demonstrating the establishment of immunological memory. Furthermore, we observed significantly more IFNγ spots by ELISpot analysis from $CD8^+$ T cells isolated from KPAR tumours treated with anti-CTLA-4 compared to isotype control when pulsing with the eMLV envelope peptide, indicating that eMLV-specific T cells expand in response to immunotherapy (Supplementary Fig. 8B). This was important for the therapeutic efficacy of ICB as, in contrast to parental KPAR tumours, anti-CTLA-4 failed to result in long-term durable regression of *Emv2*$^{-/-}$ KPAR subcutaneous tumours (Supplementary Fig. 8C).

Flow cytometry analysis of subcutaneous tumours treated with anti-CTLA-4 or anti-PD-1 demonstrated that only anti-CTLA-4 treatment effectively depleted $Foxp3^+$ Tregs (Fig. 5C), resulting in an increase in the ratio of $CD8^+$ and $CD4^+$ effector T cells to Tregs (Supplementary Fig. 8D), as previously reported (28). Anti-CTLA-4 treatment also led to an increase in the frequency of effector memory and PD-1^+ $CD8^+$ T cells in tumours (Fig. 5D). To assess whether the sensitivity to ICB was dependent on the anatomic site of tumour growth, as previously shown (29), we also treated orthotopic KPAR lung tumours with anti-PD-1, anti-CTLA-4 or a combination of both. KPAR cells were injected intravenously into mice which were subsequently treated once lung tumours were detected by micro-CT. In contrast to subcutaneous tumours, orthotopic tumours responded to both anti-CTLA-4 and anti-PD-1 monotherapies, resulting in a significant increase in the survival of tumour-bearing mice (Fig. 5E). However, the response to anti-PD1 was substantially greater, resulting in long-term responses in a subset of mice as a monotherapy or in combination with anti-CTLA-4.

Downloaded from http://aacrjournals.org/cancerres/article-pdf/doi/10.1158/0008-5472.CAN-22-0325/3186457/can-22-0325.pdf by University College of London user on 08 August 2022

Immunohistochemistry staining demonstrated that both anti-PD-1 and anti-CTLA-4 therapy increased the infiltration of $CD8^+$ T cells into the tumour (Fig. 5F, and Supplementary Fig. 8E), however this increase was greater in anti-PD-1 treated mice. In contrast to subcutaneous tumours, anti-CTLA-4 treatment failed to deplete $Foxp3^+$ Tregs in orthotopic tumours (Fig. 5G, and Supplementary Fig. 8F). Furthermore, the majority of $CD4^+$ T cells in subcutaneous tumours were Tregs whilst in orthotopic tumours $CD4^+$ effector T cells were more abundant (Supplementary Fig. 8G).

To summarise, KPAR tumours were sensitive to anti-PD-1 or anti-CTLA-4 immune checkpoint blockade therapy, the response to which was dependent on the site of tumour growth.

Generation of $KPAR^{G12C}$ cells to assess the immunomodulatory properties of $KRAS^{G12C}$ inhibitors

The recently developed class of $KRAS^{G12C}$ inhibitors has been shown to promote anti-tumour immune responses in the immunogenic $CT26^{G12C}$ model of colorectal cancer (7). To test the effect of $KRAS^{G12C}$ inhibitors in the KPAR lung cancer model we used prime-editing technology to generate the $KPAR^{G12C}$ cell line. WES revealed that KPAR cells were homozygous for $KRAS^{G12D}$ so we edited both alleles to $KRAS^{G12C}$ using prime editing technology (Supplementary Fig. 9A). Cell-viability assays demonstrated that $KPAR^{G12C}$ cells showed impaired viability in response to treatment with AZ-8037, a recently described $KRAS^{G12C}$ inhibitor (30) (Supplementary Fig. 9B). Furthermore, immunoblotting revealed that AZ-8037 inhibited pERK in $KPAR^{G12C}$ cells (Supplementary Fig. 9C). To assess whether $KRAS^{G12C}$ inhibition could stimulate anti-tumour immunity *in vivo* we tested the response of $KPAR^{G12C}$ subcutaneous tumours to AZ-8037 in both immune-competent and *Rag1*$^{-/-}$ mice. Vehicle-treated $KPAR^{G12C}$ tumours grew slower in immune-competent mice compared to *Rag1*$^{-/-}$ mice, similarly to what we observed with the parental KPAR tumours (Fig. 6A). AZ-8037 treatment caused marked tumour regression in both immune-competent and *Rag1*$^{-/-}$ mice, however the response was more durable in immune-competent mice as all tumours remained responsive during the duration of treatment whilst tumours in *Rag1*$^{-/-}$ mice began to grow back before termination of treatment (Fig. 6A, Supplementary Fig. 10A). Furthermore, after the treatment was terminated one of the six treated mice showed a durable cure (Fig. 6B).

Downloaded from http://aacrjournals.org/cancerres/article-pdf/doi/10.1158/0008-5472.CAN-22-0325/3186457/can-22-0325.pdf by University College of London user on 08 August 2022

We also used CRISPR technology to edit the KPB6 cell line, which harbours a wildtype KRAS and $KRAS^{G12D}$ allele, to generate the $KPB6^{G12C}$ cell line which lost the wildtype allele by indel generation and contained a $KRAS^{G12C}$ allele (Supplementary Fig. 9D). Cell-viability assays and immunoblotting demonstrated that $KPB6^{G12C}$ cells were sensitive to AZ-8037 (Supplementary Fig. 9E-F). In contrast to $KPAR^{G12C}$ tumours, the response of $KPB6^{G12C}$ tumours to AZ-8037 was comparable in immune-competent and *Rag1*$^{-/-}$ mice (Fig. 6C, Supplementary Fig. 10B), with tumours beginning to lose responsiveness before treatment ended, and then growing back rapidly after the cessation of treatment with no long-term responses achieved (Fig. 6D).

Given that adaptive immunity contributes to the efficacy of $KRAS^{G12C}$ inhibition in KPAR tumours, we next wanted to assess the effects of $KRAS^{G12C}$ inhibition on the tumour microenvironment. qPCR analysis of orthotopic $KPAR^{G12C}$ tumours revealed that $KRAS^{G12C}$ inhibition induced a pro-inflammatory microenvironment with increased antigen presentation, cytokine production, interferon signalling, immune cell infiltration and T cell activation (Fig. 6E). ELISA analysis of tumour lysates validated the increased expression of T-cell chemoattractants (CXCL9 and CXCL10) upon $KRAS^{G12C}$ inhibition (Supplementary Fig. 10C). Given that $KRAS^{G12C}$ inhibition promoted anti-tumour immunity we next asked whether this would improve the efficacy of immune checkpoint blockade. Mice bearing subcutaneous $KPAR^{G12C}$ tumours were treated either with anti-PD-1, AZ-8037 or a combination of both. Similar to parental tumours, $KPAR^{G12C}$ tumours showed little response to anti-PD-1, and whilst AZ-8037 treatment led to the regression of all tumours, no durable responses were achieved and they all grew back after treatment was withdrawn (Fig. 6F). In contrast, the combination of AZ-8037 and anti-PD-1 led to the durable cures in 50% of mice which remained tumour-free until 100 days, at which point they were culled (Supplementary Fig. 10D). Furthermore, these mice successfully rejected secondary tumours when re-challenged on the opposite flank (Supplementary Fig. 10D), indicating the generation of long-term immune memory.

These results suggest the efficacy of $KRAS^{G12C}$ inhibition in the immunogenic KPAR model was partially due to the generation of an adaptive anti-tumour immune response which could result in durable regressions in immune-competent hosts, especially in combination with ICB.

Downloaded from http://aacrjournals.org/cancerres/article-pdf/doi/10.1158/0008-5472.CAN-22-0325/3186457/can-22-0325.pdf by University College of London user on 08 August 2022

DISCUSSION

There is a need for improved models of lung cancer that are immunogenic to enable us to better understand the interplay between the tumour and the immune system and assess the efficacy of novel therapeutic interventions. We and others have tried several approaches to make lung cancer GEMMs more immunogenic, including treating KP mice with carcinogens. However, these strategies have failed to generate immunogenic tumours that grew differentially in immune-competent and immune-deficient backgrounds or responded to immune checkpoint blockade. In this study, APOBEC3B expression only moderately increased the tumour mutational burden in KP and urethane-induced lung tumours and was not sufficient to make these tumours immunogenic. The lack of substantial numbers of APOBEC3B-induced mutations in these models was potentially a consequence of a detrimental impact of APOBEC3B expression during early stages of tumour development, which is reflected by the downregulation of A3Bi expression in both KP and urethane-induced lung tumours. Indeed, expression of APOBEC3B in an $EGFR^{L858R}$-driven model of lung cancer has also been shown to be detrimental to tumour initiation (31). The development of a KP model with temporal regulation of APOBEC3B could help address this limitation.

Despite containing many more clonal exonic mutations than A3Bi-expressing KP tumours, urethane-induced lung tumours were also refractory to ICB. The long latency of urethane-induce lung tumours may provide ample time for the elimination of immunogenic clones or the establishment of immune tolerance. Such results highlight the potential differences in the ability of transplantable and autochthonous models to induce adaptive immune responses or immune tolerance, as previously reported (32), and raises the possibility that autochthonous models could be sensitised to ICB with specific combination therapies. Alternatively, a higher number of somatic mutations than achieved here may be required. Indeed, peptide screens of human tumour samples have revealed that only a minority of mutations result in neoantigens that are recognised by TILs (33). Furthermore, neither APOBEC3B nor urethane mimic tobacco-induced C>A mutations which are prevalent in human LUAD. Such a model would be physiologically relevant and would be useful for studying how different mutational processes affect tumour development and anti-tumour immunity. However, the inability of tobacco carcinogens to efficiently drive lung adenocarcinoma in C57BL/6 mice limits the utility of this approach. Together these results highlight the

Downloaded from http://aacrjournals.org/cancerres/article-pdf/doi/10.1158/0008-5472.CAN-22-0325/3186457/can-22-0325.pdf by University College of London user on 08 August 2022

limitations of autochthonous models of lung cancer which fail to induce anti-tumour immune responses.

Given the limitations of autochthonous models, most preclinical studies of immunotherapy utilise transplantable syngeneic cell lines. The most commonly used mouse cancer cell lines used for syngeneic transplantation that are sensitive to immunotherapy are the colorectal carcinoma cell line CT26 and renal cancer cell line RENCA, with many other commonly used lines such as MC38 colorectal cancer, B16-F10 melanoma and 4T1 breast cancer being largely refractory to immune checkpoint blockade (34). The most commonly used murine lung cancer cell line for orthotopic preclinical studies is the 3LL cell line, also referred to as LL/2 or LLC1, and derivative variants, which originate from a spontaneous Lewis lung carcinoma tumour in a C57BL/6 mouse that has been serially passaged in immune-competent mice, leading to a highly immune evasive phenotype (34). It has activating mutations in both KRAS and NRAS (35), however these tumours are refractory to ICB (36), largely due to their ability to generate a very immunosuppressive tumour microenvironment rather than a lack of tumour neoantigens, and therefore do not make a suitable model for studying the response to novel therapy combinations in an immune-hot tumour microenvironment context. Another transplantable mouse lung cancer cell line, CMT-167, which also originated from a spontaneous tumour, has been characterised as $KRAS^{G12V}$ mutant and found to be responsive to immunotherapy (29). An immunogenic transplantable lung cancer cell line has also been generated using tobacco carcinogens (37), mimicking the mutational processes that occur in the majority of human LUAD patients, however its utility is limited by its establishment on an FVB/N background.

In this study, we established the KPAR cell line from a single-cell clone of a KP tumour expressing APOBEC3B which had developed in an immune-deficient background and therefore could not undergo immune-editing. We used the KPAR cell line as an orthotopic transplantable model of lung cancer and demonstrated that this model was immunogenic, stimulating anti-tumour immune responses which sensitised tumours to immune checkpoint blockade. Although the cell line was generated from the KP-A3Bi GEMM, it did not possess a substantial number of new mutations and instead, we observed anti-tumour immune responses directed against derepressed endogenous retroviral proteins which contributed to the efficacy of immunotherapy. These observations suggest APOBEC3B-mediated mutagenesis did not directly

Downloaded from http://aacrjournals.org/cancerres/article-pdf/doi/10.1158/0008-5472.CAN-22-0325/3186457/can-22-0325.pdf by University College of London user on 08 August 2022

contribute to the immunogenicity of the KPAR cell line, however other mechanisms such as induction of chromosomal instability, as previously reported (19), cannot be ruled out. Several immunogenic murine cancer cell lines, including CT26 (38), B16 and MC38 (39), have been shown to express endogenous retroviral proteins which can act as antigens that are recognised by T cells. As demonstrated recently, forced expression of endogenous retroviral proteins is sufficient to render murine cancer cell lines immunogenic (40) and therefore represents an attractive approach for the generation of immunogenic models. Anti-tumour immune responses have also been observed against human endogenous retroviruses in melanoma (41) and breast cancer (41), however the relevance of these antigens in lung cancer remains unclear. Nevertheless, elevated expression of a tumour-associated antigen may better model anti-tumour immune responses that occur in human cancers compared to the expression of strong foreign antigens such as ovalbumin, luciferase (9) or lymphocytic choriomeningitis virus glycoprotein (42). Indeed, the expression of these antigens in KP lung cancer cells results in the rejection of transplanted cells or the selection of clones that have lost antigen expression (9).

Most studies of immunotherapy utilising transplantable cell lines involve subcutaneous transplantation into syngeneic immune-competent mice. We observed a striking difference in the response to anti-PD-1 or anti-CTLA-4 in subcutaneous versus orthotopic tumours, as previously demonstrated for PD-1/PD-L1 blockade (29). Subcutaneous KPAR tumours responded to anti-CTLA4 but were refractory to anti-PD-1, as observed in an immunogenic melanoma model (43). Anti-CTLA-4 can induce tumour regression through the depletion of Tregs in subcutaneous tumours(28) which we observed in KPAR subcutaneous tumours. The high ratio of $Foxp3^+$ Tregs to $CD4^+$ effector T cells in subcutaneous tumours may explain why they are refractory to PD-1 blockade. Conversely, the reduced fraction of Tregs in orthotopic tumours may explain the minimal response to CTLA-4 blockade. Together these results highlight the importance of studying tumours in their tissue of origin when assessing responses to ICB, with orthotopic tumours likely to yield more directly clinically relevant information than subcutaneous tumours.

The recently developed $KRAS^{G12C}$ specific inhibitors have produced outstanding responses in NSCLC (44). A recent study showed that these inhibitors could promote T cell responses through increased IFNγ signalling in the immunogenic $CT26^{G12C}$ colon cancer transplantable model (7,45). Similar to what was shown in these studies,

Downloaded from http://aacrjournals.org/cancerres/article-pdf/doi/10.1158/0008-5472.CAN-22-0325/3186457/can-22-0325.pdf by University College of London user on 08 August 2022

we observed profound changes in the tumour microenvironment in response to $KRAS^{G12C}$ inhibition, indicative of enhanced anti-tumour immune responses. Furthermore, the tumour regression we observed after $KRAS^{G12C}$ inhibition in $KPAR^{G12C}$ tumours was more profound in immune-competent mice; however, this was not the case for non-immunogenic $KPB6^{G12C}$ tumours. This result suggests that the efficacy of $KRAS^{G12C}$ inhibitors is partially due to the engagement of the adaptive immune system in immune-hot tumours. Using the KPAR model, we demonstrated the superior efficacy of combining immunotherapy with $KRAS^{G12C}$ inhibition which may potentially overcome the acquired resistance anticipated following this novel targeted therapy (46).

In conclusion, we have created a novel model of immunogenic KRAS-driven lung adenocarcinoma, which we anticipate will contribute to the development of new combinations of therapies, including those involving immune checkpoint blockade and $KRAS^{G12C}$ inhibition.

Downloaded from http://aacrjournals.org/cancerres/article-pdf/doi/10.1158/0008-5472.CAN-22-0325/3186457/can-22-0325.pdf by University College of London user on 08 August 2022

ACKNOWLEDGEMENTS

We thank the science technology platforms at the Francis Crick Institute including Biological Resources, Scientific Computing, Bioinformatics and Biostatistics, Flow Cytometry, Experimental Histopathology, and Cell Services. We also thank Colleen Forster and Gerard O'Sullivan for assistance with immunohistochemistry and pathology, Yasuhiko Kawakami for sharing CMV-Cre animals, and Brian Dunnette for expertise with the Aperio ScanScope XT at the University of Minnesota.

Funding: This work was supported by funding to J.D. from the Francis Crick Institute—which receives its core funding from Cancer Research UK (FC001070), the UK Medical Research Council (FC001070), and the Wellcome Trust (FC001070)—from the European Research Council Advanced Grant RASImmune, and from a Wellcome Trust Senior Investigator Award 103799/Z/14/Z. The *A3Bi* minigene model was developed with support from the National Cancer Institute P01-CA234228 (RSH), Team Judy (RSH), Randy Shaver Cancer Research and Community Fund (RSH), University of Minnesota Masonic Cancer Center, and College of Biological Sciences (RSH). RSH is the Ewing Halsell President's Council Distinguished Chair at University of Texas San Antonio and an Investigator of the Howard Hughes Medical Institute. S.C.T received funding from the European Union's Horizon 2020 research and innovation programme under the Marie Sklodowska-Curie grant agreement No 703228.

Competing interests: J.D. has acted as a consultant for AstraZeneca, Bayer, Jubilant, Theras, Vividion and Novartis. S.R. is an employee of AstraZeneca. C.S. receives grant support from Archer Dx, AstraZeneca, Boehringer–Ingelheim and Ono Pharmaceutical; has consulted for AstraZeneca, Bicycle Therapeutics, Celgene, Genentech, GRAIL, GSK, Illumina, Medicxi, MSD, Novartis and the Sarah Cannon Research Institute; receives grant support and has consulted for Bristol Myers Squibb, Pfizer and Roche–Ventana; is an advisory board member and is involved in trials sponsored by AstraZeneca; has stock options in Epic Sciences, GRAIL; and has stock options and is a co-founder of Achilles Therapeutics. The other authors declare that they have no competing interests.

Author contributions: S.C.T, J.B., E.K.L., G.K., R.S.H. and J.D. designed the study, interpreted the results and wrote the manuscript. S.C.T, J.B., P.R.C., M.M-A., M.A.C., S.R., E.M., K.N. and D.H. performed the biochemical experiments, C.M. assisted with *in vivo* studies, P.P.A., C.D., A.S.B., S.P. performed pathological studies, S.H. and

Downloaded from http://aacrjournals.org/cancerres/article-pdf/doi/10.1158/0008-5472.CAN-22-0325/3186457/can-22-0325.pdf by University College of London user on 08 August 2022

P.E. performed bioinformatics analyses, R.S.H. designed the A3B knock-in model, supervised validation studies, contributed support and reagents, obtained funding, and edited the manuscript. E.K.L. created DNA constructs, performed validation studies, and conducted full body expression experiments. W.L.B., L.K.L., and C.D. provided technical and logistical assistance. R.I.V. provided statistical analysis. All authors contributed to manuscript revision and review.

Downloaded from http://aacrjournals.org/cancerres/article-pdf/doi/10.1158/0008-5472.CAN-22-0325/3186457/can-22-0325.pdf by University College of London user on 08 August 2022

REFERENCES

1. Bray F, Ferlay J, Soerjomataram I, Siegel RL, Torre LA, Jemal A. Global cancer statistics 2018: GLOBOCAN estimates of incidence and mortality worldwide for 36 cancers in 185 countries. CA Cancer J Clin. 2018;68:394–424.
2. Siegel RL, Miller KD, Jemal A. Cancer statistics, 2020. CA Cancer J Clin. 2020;70:7–30.
3. Collisson EA, Campbell JD, Brooks AN, Berger AH, Lee W, Chmielecki J, et al. Comprehensive molecular profiling of lung adenocarcinoma. Nature. Nature Publishing Group; 2014;511:543–50.
4. Blumenschein GR, Smit EF, Planchard D, Kim DW, Cadranel J, De Pas T, et al. A randomized phase II study of the MEK1/MEK2 inhibitor trametinib (GSK1120212) compared with docetaxel in KRAS-mutant advanced non-small-cell lung cancer (NSCLC). Ann Oncol. 2015;26:894–901.
5. Borghaei H, Paz-Ares L, Horn L, Spigel DR, Steins M, Ready NE, et al. Nivolumab versus docetaxel in advanced nonsquamous non-small-cell lung cancer. N Engl J Med. 2015;373:1627–39.
6. Coelho MA, de Carné Trécesson S, Rana S, Zecchin D, Moore C, Molina-Arcas M, et al. Oncogenic RAS signaling promotes tumor immunoresistance by stabilizing PD-L1 mRNA. Immunity. 2017;47:1083–99.
7. Canon J, Rex K, Saiki AY, Mohr C, Cooke K, Bagal D, et al. The clinical KRAS (G12C) inhibitor AMG 510 drives anti-tumour immunity. Nature. 2019;575:217–23.
8. Pfirschke C, Engblom C, Rickelt S, Cortez-Retamozo V, Garris C, Pucci F, et al. Immunogenic Chemotherapy Sensitizes Tumors to Checkpoint Blockade Therapy. Immunity [Internet]. Elsevier Inc.; 2016;44:343–54. Available from: http://dx.doi.org/10.1016/j.immuni.2015.11.024
9. DuPage M, Cheung AF, Mazumdar C, Winslow MM, Bronson R, Schmidt LM, et al. Endogenous T cell responses to antigens expressed in lung adenocarcinomas delay malignant tumor progression. Cancer Cell [Internet]. Elsevier Inc.; 2011;19:72–85. Available from: http://dx.doi.org/10.1016/j.ccr.2010.11.011
10. McFadden DG, Politi K, Bhutkar A, Chen FK, Song X, Pirun M, et al. Mutational landscape of EGFR- , MYC- , and Kras- driven genetically engineered mouse models of lung adenocarcinoma. Proc Natl Acad Sci [Internet]. 2016;113:6409–17. Available from: http://www.pnas.org/lookup/doi/10.1073/pnas.1613601113
11. Joshi NS, Akama-Garren EH, Lu Y, Lee DY, Chang GP, Li A, et al. Regulatory T cells in tumor-associated tertiary lymphoid structures suppress anti-tumor T cell responses. Immunity [Internet]. Elsevier Inc.; 2015;43:579–90. Available from: http://dx.doi.org/10.1016/j.immuni.2015.08.006
12. Burns MB, Temiz NA, Harris RS. Evidence for APOBEC3B mutagenesis in multiple human cancers. Nat Genet. Nature Publishing Group; 2013;45:977–

Downloaded from http://aacrjournals.org/cancerres/article-pdf/doi/10.1158/0008-5472.CAN-22-0325/3186457/can-22-0325.pdf by University College of London user on 08 August 2022

83.

13. DuPage M, Dooley AL, Jacks T. Conditional mouse lung cancer models using adenoviral or lentiviral delivery of Cre recombinase. Nat Protoc. 2009;4:1064–72.
14. Brown WL, Law EK, Carpenter MA, Argyris PP, Levin-Klein R, Ranum AN, et al. A rabbit monoclonal antibody against the antiviral and cancer genomic DNA mutating enzyme APOBEC3B. Antibodies (Basel). 2019;8.
15. Pfaffl MW. A new mathematical model for relative quantification in real-time RT–PCR. Nucleic Acids Res. 2001;29:2002–7.
16. Jackson EL, Olive KP, Tuveson DA, Bronson R, Crowley D, Brown M, et al. The differential effects of mutant p53 alleles on advanced murine lung cancer. Cancer Res. 2005;65:10280–8.
17. Ebert PJR, Cheung J, Yang Y, McNamara E, Hong R, Moskalenko M, et al. MAP Kinase Inhibition Promotes T Cell and Anti-tumor Activity in Combination with PD-L1 Checkpoint Blockade. Immunity [Internet]. Elsevier Inc.; 2016;44:609–21. Available from: http://dx.doi.org/10.1016/j.immuni.2016.01.024
18. Roberts SA, Lawrence MS, Klimczak LJ, Grimm SA, Fargo D, Stojanov P, et al. An APOBEC cytidine deaminase mutagenesis pattern is widespread in human cancers. Nat Genet. Nature Publishing Group; 2013;45:970–6.
19. Venkatesan S, Angelova M, Puttick C, Zhai H, Caswell DR, Lu WT, et al. Induction of APOBEC3 exacerbates DNA replication stress and chromosomal instability in early breast and lung cancer evolution. Cancer Discov. 2021;11:2456–73.
20. De Bruin EC, McGranahan N, Mitter R, Salm M, Wedge DC, Yates L, et al. Spatial and temporal diversity in genomic instability processes defines lung cancer evolution. Science (80-). 2014;346:251–6.
21. Swanton C, McGranahan N, Starrett GJ, Harris RS. APOBEC Enzymes: Mutagenic Fuel for Cancer Evolution and Heterogeneity. Cancer Discov. 2015;5:704–12.
22. Westcott PMK, Halliwill KD, To MD, Rashid M, Rust AG, Keane TM, et al. The mutational landscapes of genetic and chemical models of Kras-driven lung cancer. Nature [Internet]. Nature Publishing Group; 2015;517:489–92. Available from: http://www.nature.com/doifinder/10.1038/nature13898
23. Li S, MacAlpine DM, Counter CM. Capturing the primordial Kras mutation initiating urethane carcinogenesis. Nat Commun [Internet]. Springer US; 2020;11. Available from: http://dx.doi.org/10.1038/s41467-020-15660-8
24. Wolf Y, Bartok O, Patkar S, Eli GB, Cohen S, Litchfield K, et al. UVB-Induced Tumor Heterogeneity Diminishes Immune Response in Melanoma. Cell. 2019;179:219–35.
25. McGranahan N, Furness AJS, Rosenthal R, Ramskov S, Lyngaa R, Saini SK, et al. Clonal neoantigens elicit T cell immunoreactivity and sensitivity to immune checkpoint blockade. Science (80-). 2016;351:1463–9.
26. Ottina E, Levy P, Eksmond U, Merkenschlager J, Young GR, Roels J, et al.

Downloaded from http://aacrjournals.org/cancerres/article-pdf/doi/10.1158/0008-5472.CAN-22-0325/3186457/can-22-0325.pdf by University College of London user on 08 August 2022

Restoration of endogenous retrovirus infectivity impacts mouse cancer models. Cancer Immunol Res. 2018;6:1292–300.

27. Kassiotis G, Stoye JP. Immune responses to endogenous retroelements: Taking the bad with the good. Nat Rev Immunol. Nature Publishing Group; 2016;16:207–19.

28. Simpson TR, Li F, Montalvo-Ortiz W, Sepulveda MA, Bergerhoff K, Arce F, et al. Fc-dependent depletion of tumor-infiltrating regulatory T cells co-defines the efficacy of anti-CTLA-4 therapy against melanoma. J Exp Med. 2013;210:1695–710.

29. Li HY, Mcsharry M, Bullock B, Nguyen TT, Kwak J, Poczobutt JM, et al. The tumor microenvironment regulates sensitivity of murine lung tumors to PD-1 / PD-L1 antibody blockade. Cancer Immunol Res. 2017;5:767–78.

30. Kettle JG, Bagal SK, Bickerton S, Bodnarchuk MS, Breed J, Carbajo RJ, et al. Structure-Based Design and Pharmacokinetic Optimization of Covalent Allosteric Inhibitors of the Mutant GTPase KRASG12C. J Med Chem. 2020;63:4468–83.

31. Mayekar MK, Caswell DR, Vokes NI, Law EK, Wu W, Hill W, et al. Targeted cancer therapy induces APOBEC fuelling the evolution of drug resistance. bioRxiv. 2020;

32. Wisdom AJ, Mowery YM, Hong CS, Himes JE, Nabet BY, Qin X, et al. Single cell analysis reveals distinct immune landscapes in transplant and primary sarcomas that determine response or resistance to immunotherapy. Nat Commun [Internet]. Springer US; 2020;11:6410. Available from: http://dx.doi.org/10.1038/s41467-020-19917-0

33. Robbins PF, Lu YC, El-Gamil M, Li YF, Gross C, Gartner J, et al. Mining exomic sequencing data to identify mutated antigens recognized by adoptively transferred tumor-reactive T cells. Nat Med. Nature Publishing Group; 2013;19:747–52.

34. Mosely SIS, Prime JE, Sainson RCA, Koopmann J-O, Wang DYQ, Greenawalt DM, et al. Rational selection of syngeneic preclinical tumor models for immunotherapeutic drug discovery. Cancer Immunol Res. 2017;5:29–41.

35. Molina-Arcas M, Moore C, Rana S, Van Maldegem F, Mugarza E, Romero-Clavijo P, et al. Development of combination therapies to maximize the impact of KRAS-G12C inhibitors in lung cancer. Sci Transl Med. 2019;11:eaaw7999.

36. Mugarza E, Maldegem F van, Boumelha J, Moore C, Rana S, Sopena ML, et al. Therapeutic KRAS^{G12C} inhibition drives effective interferon-mediated anti-tumour immunity in immunogenic lung cancers. bioRxiv [Internet]. 2021; Available from: https://www.biorxiv.org/content/10.1101/2021.10.18.464819v1%0Ahttps://www.biorxiv.org/content/10.1101/2021.10.18.464819v1.abstract

37. Stabile LP, Kumar V, Gaither-Davis A, Huang EH, Vendetti FP, Devadassan P, et al. Syngeneic tobacco carcinogen-induced mouse lung adenocarcinoma model exhibits PD-L1 expression and high tumor mutational burden. JCI Insight. 2021;6:e145307.

38. Huang AYC, Gulden PH, Woods AS, Thomas MC, Tong CD, Wang W, et al.

Downloaded from http://aacrjournals.org/cancerres/article-pdf/doi/10.1158/0008-5472.CAN-22-0325/3186457/can-22-0325.pdf by University College of London user on 08 August 2022

The immunodominant major histocompatibility complex class I-restricted antigen of a murine colon tumor derives from an endogenous retroviral gene product. Proc Natl Acad Sci U S A. 1996;93:9730–5.

39. Yang J, Perry-Lalley D. The Envelope Protein of an Endogenous Murine Retrovirus Is a Tumor-Associated T-Cell Antigen for Multiple Murine Tumors. J Immunother. 2000;23:177–83.

40. Ottina E, Panova V, Doglio L, Kazachenka A, Cornish G, Kirkpatrick J, et al. E3 ubiquitin ligase HECTD2 mediates melanoma progression and immune evasion. Oncogene. 2021;40:5567–78.

41. Schiavetti F, Thonnard J, Colau D, Boon T, Coulie PG. A human endogenous retroviral sequence encoding an antigen recognized on melanoma by cytolytic T lymphocytes. Cancer Res. 2002;62:5510–6.

42. Damo M, Fitzgerald B, Lu Y, Nader M, William I, Cheung JF, et al. Inducible de novo expression of neoantigens in tumor cells and mice. Nat Biotechnol [Internet]. Springer US; 2021;39:64–73. Available from: http://dx.doi.org/10.1038/s41587-020-0613-1

43. Lelliott EJ, Cullinane C, Martin CA, Walker R, Ramsbottom KM, Souza-Fonseca-Guimaraes F, et al. A novel immunogenic mouse model of melanoma for the preclinical assessment of combination targeted and immune-based therapy. Sci Rep. 2019;9:1225.

44. Hong DS, Fakih MG, Strickler JH, Desai J, Durm GA, Shapiro GI, et al. KRAS G12C Inhibition with Sotorasib in Advanced Solid Tumors. N Engl J Med. 2020;383:1207–17.

45. Briere DM, Li S, Calinisan A, Sudhakar N, Aranda R, Hargis L, et al. The KRAS^{G12C} Inhibitor MRTX849 Reconditions the Tumor Immune Microenvironment and Sensitizes Tumors to Checkpoint Inhibitor Therapy. Mol Cancer Ther [Internet]. 2021;20:975 LP – 985. Available from: http://mct.aacrjournals.org/content/20/6/975.abstract

46. Xue JY, Zhao Y, Aronowitz J, Mai TT, Vides A, Qeriqi B, et al. Rapid non-uniform adaptation to conformation-specific KRAS(G12C) inhibition. Nature [Internet]. Springer US; 2020;577:421–5. Available from: http://dx.doi.org/10.1038/s41586-019-1884-x

Downloaded from http://aacrjournals.org/cancerres/article-pdf/doi/10.1158/0008-5472.CAN-22-0325/3186457/can-22-0325.pdf by University College of London user on 08 August 2022

Downloaded from http://aacrjournals.org/cancerres/article-pdf/doi/10.1158/0008-5472.CAN-22-0325/3186457/can-22-0325.pdf by University College of London user on 08 August 2022

Figure legends

Figure 1. The KP mouse model of lung adenocarcinoma is not immunogenic
(A) Tumour volume change over two weeks in KP;*Rag2*$^{+/-}$ (n=5) and KP;*Rag2*$^{-/-}$ mice (n=4). Data are mean per mouse (large symbols) ± SEM, small symbols represent individual tumours. Mann-Whitney test of mean per mouse; ns P>0.05.
(B) Tumour burden quantified using H&E sections from KP;*Rag2*$^{+/-}$ (n=7) and KP;*Rag2*$^{-/-}$ mice (n=8) 15 weeks after tumour initiation. Data are mean ± SEM. Unpaired, two-tailed Student's t-test; ns P>0.05.
(C) Schematic of KP tumour induction and treatment schedule. Cre-expressing adenovirus was delivered intratracheally and mice were regularly scanned by micro-CT. 12 weeks after tumour initiation, tumour-bearing mice were treated three times (d0, d4 and d8) intraperitoneally with 10mg/kg anti-PD-L1 and 5mg/kg anti-CTLA-4 or corresponding isotype control (IgG Ctl). Tumour growth and survival were monitored until the experimental endpoints.
(D) Tumour volume change in KP-tumour-bearing mice treated as in (C) Mice were scanned 2 weeks after the pre-treatment scan, IgG Ctl (n=7) and anti-PD-L1 + anti-CTLA-4 (n=7). Data are mean per mouse (large symbols) ± SEM, small symbols represent individual tumours. Mann-Whitney test of mean per mouse; ns P>0.05.
(E) Representative micro-CT scans of mice treated as in (C). Red arrows indicate tumours.
(F) Kaplan-Meier survival analysis of KP-tumour-bearing mouse survival treated as in (C). Log-rank (Mantel-Cox) test; ns P>0.05

Figure 2. APOBEC3B expression induces subclonal mutations but does not render autochthonous tumours immunogenic
(A) Distribution of log2 non-synonymous/synonymous mutation ratio of APOBEC mutations or other types of mutation in LUAD (TCGA).
(B) Distribution of A3Bi positive cells per lung tumour in the KPA model estimated by immunohistochemistry.
(C) Immunohistochemistry of APOBEC3B staining in four KPA tumours showing different levels of APOBEC3B expression. Scale bar represents 100μm.

(D)Tumour grade proportion in the KP and KPA models. Percentage per model, upper and lower limit, Chi-square test p-value, n=5 mice per group; ** P≤0.01.
(E) Percentage of mitotic cells in KP and KPA tumours estimated by histopathology. Light grey dots represent individual tumours. Mean per group (large symbols), ±SEM, n=5 mice per group. One-way ANOVA of mean per group, FDR 0.05; * P≤0.05.
(F) Quantification of immunohistochemistry staining for CD8 in KP and KPA tumours. Light grey dots represent individual tumours. Mean per group (large symbols), ±SEM, n=5 mice per group. One-way ANOVA of mean per group, FDR 0.05; ** P≤0.01.
(G) Immunohistochemistry of CD8 in lung tumours from KP and KPA models. Scale bar represents 100μm.
(H) Tumour volume change in KP- and KPA-tumour-bearing mice treated four times (d0, d3, d7 and d10) with 200μg of anti-PD-1 and 200μg of anti-CTLA-4. Mice were scanned 2 weeks after the pre-treatment scan, KP (n=4) and KPA (n=7). Data are mean (large symbols) ± SEM, small symbols represent individual tumours. Mann-Whitney test; ns P>0.05.
(I-J) Mean exonic SNV count ±SD (I) and neoantigen count ±SD (J) in KP (n=5 tumours) and KPA (n=3 tumours) broken down into clonal and subclonal. Unpaired, two-tailed Student's t-test performed on mean of all SNVs or neoantigen count; * P≤0.05, ** P≤0.01. Peptides with a rank threshold of <2 or <0.5 were designated as weak or strong MHC-I binders, respectively.
(K) Expression of *A3Bi* by qPCR in paired normal-adjacent tissue and tumour of UrA3Bi (n=7 tumours from 4 mice, squares), each symbol represents one tumour or adjacent tissue. Relative expression is normalised on the mean expression of *Sdha*, *Tbp* and *Actb*. Two-tailed paired t-test; ** P≤0.01
(L) Proportion of tumour grades evaluated from H&E staining of tumour-bearing lungs in Ur (n=8 mice) and UrA3Bi (n=8 mice) mice. Chi-square test; ** P≤0.01.
(M) Tumour volume change in UrA3Bi mice treated as in (H) (n=2 mice) or corresponding isotype control (n=2 mice). Mice were scanned 2 weeks after the pre-treatment scan. Data are mean per mouse (large symbols) ± SEM, small symbols represent individual tumours. Mann-Whitney test; ns P>0.05.
(N-O) Mean total exonic SNV count ±SD (M) and neoantigen count ±SD (N) in Ur (n=3 tumours) and UrA3B (n=6 tumours). Unpaired t-test, two-tailed performed on mean of all SNVs or neoantigen count; ns P>0.05

Figure 3. Generation of a novel immunogenic cell line KPAR1.3
(A) mRNA expression by qPCR of *A3Bi* in KPA and KPAR autochthonous tumours, parental cells and sub-clones. Relative expression is normalised to the mean expression of *Sdha*, *Tbp* and *Hsp90ab1*.

Downloaded from http://aacrjournals.org/cancerres/article-pdf/doi/10.1158/0008-5472.CAN-22-0325/3186457/can-22-0325.pdf by University College of London user on 08 August 2022

(B) Growth of KPAR cells transplanted subcutaneously into syngeneic immune-competent and *Rag1*$^{-/-}$ mice. Data are mean tumour volumes ± SEM, n=5 mice per group (KPAR1.3 and KPAR1.5) and n=4 mice per group (KPAR1.1). Two-way ANOVA; ns P>0.05, *** P≤0.001
(C) Frequency of exonic mutations in an autochthonous KPAR tumour, the KPAR parental cell line and the KPAR1.1, KPAR1.3 and KPAR1.5 single-cell clones, estimated par whole-exome sequencing.
(D) Frequency of predicted neoantigens identified using NetMHC4.0. Peptides with a rank threshold of <2 or <0.5 were designated as weak or strong MHC-I binders, respectively.
(E) IFNγ ELISPOT analysis of splenocytes isolated from KPAR1.3 tumour-bearing mice and pulsed with predicted strong neoantigens (SSFLCKGL and VTALYKLAL) or eMLV *env* peptide (KSPWFTTL). SINFEKL was used as a negative control. Data are mean ± SEM, n=4 mice per group. One-way ANOVA; ** P≤0.01

Figure 4. KPAR orthotopic tumours generate an adaptive immune response

(A) Immune profile of KPAR and KPB6 orthotopic tumours compared to normal lung, assessed by flow cytometry.
(B) Frequency of tumour-infiltrating T cell populations and NK cells.
(C) Percentage of effector memory CD8$^+$ (left) and CD4$^+$ (right) T cells.
(D) Quantification of PD-1, LAG-3 and TIM-3 expression on CD8$^+$ (left) and CD4$^+$ (right) T cells.
(E) Representative plot of PD-1 and LAG-3 expression on CD8$^+$ T cells.
(F) Frequency of PDL1$^+$ macrophages, cDC1, cDC2, monocytes and neutrophils.
Tumours were analysed 21 days after transplantation. In (B)-(D) and (F), data are mean ± SEM, n=4 mice (KPB6) or 9 mice (KPAR), symbols represent pooled tumours from individual mice. Unpaired, two-tailed Student's t-test; ns P>0.05, * P≤0.05, ** P≤0.01, *** P≤0.001, **** P≤0.0001.

Figure 5. Subcutaneous and orthotopic KPAR tumours are responsive to immune checkpoint blockade

(A) Growth of KPAR subcutaneous tumours from mice treated intraperitoneally with 200µg anti-PD-1 and/or 200µg anti-CTLA-4 or corresponding isotype control (IgG Ctl) on day 10, 14, 17 and 21. Data are mean tumour volumes ± SEM, n=6 mice per group. Two-way ANOVA; ** P≤0.01, *** P≤0.001.
(B) Kaplan-Meier survival of mice from (A). The black arrow indicates the time at which mice that previously rejected the primary tumour were re-challenged on the opposite flank. Log-rank (Mantel-Cox) test; ** P≤0.01.
(C-D) Flow cytometry analysis of the frequency of Foxp3$^+$ Tregs (C), effector memory CD8$^+$ T cells (D, left) and PD-1$^+$ CD8$^+$ T cells (D, right) in subcutaneous tumours after treatment as in (A). Treatment was on day 10, 14 and 17 and mice

Downloaded from http://aacrjournals.org/cancerres/article-pdf/doi/10.1158/0008-5472.CAN-22-0325/3186457/can-22-0325.pdf by University College of London user on 08 August 2022

were culled on day 18. Data are mean ± SEM, n=5 mice per group. One-way ANOVA; ** P≤0.01, *** P≤0.001.
(E) Kaplan-Meier survival of mice treated with anti-PD-1 and/or anti-CTLA-4 after orthotopic transplantation of KPAR cells. Treatment was initiated once tumours were detectable by micro-CT and were administered twice weekly for a maximum of 3 weeks. n=6 mice (IgG Ctl, anti-PD1, anti-CTLA-4) or n=7 mice (anti-PD-1 + anti-CTLA-4). Log-rank (Mantel-Cox) test; * P≤0.05, ** P≤0.01.
(F-G) Quantification of immunohistochemistry staining for CD8 (F) and Foxp3 (G) in orthotopic KPAR lung tumours after treatment as in (E). Data are mean (large symbols) ± SEM, n=3 mice per group, small symbols represent individual tumours. One-way ANOVA; ns P>0.05, * P≤0.05, ** P≤0.01.

Figure 6. The efficacy of KRAS^{G12C} inhibition in vivo is greater in immune-competent mice
(A-B) Mean ± SEM (A) and individual (B) KPAR^{G12C} tumour volumes in immune-competent and *Rag1*$^{-/-}$ mice treated with vehicle or AZ-8037 (100mg/kg daily oral gavage). CR, complete regression. n=6 mice per group. Two-way ANOVA; *** P≤0.001, **** P≤0.0001.
(C-D) Mean ± SEM (C) and individual (D) KPB6^{G12C} tumour volumes in immune-competent and *Rag1*$^{-/-}$ mice treated as in (A). CR, complete regression. n=6 mice per group.
(E) Heatmap showing mRNA expression from qPCR of KPAR^{G12C} tumours treated for 7 days with AZ-8037 or vehicle. Gene expression is scaled across all tumours. Only genes with a significant mean difference between AZ-8037 and vehicle groups (one-way ANOVA) are shown.
(F) Individual subcutaneous KPAR^{G12C} tumour volumes in mice treated with AZ-8037 and/or 200μg anti-PD-1 or corresponding isotype control. AZ-8037 was administered daily for 4 weeks from day 14 and anti-PD-1 was administered on day 15, 18, 22 and 25. CR, complete regression. n=6 mice per group.

Downloaded from http://aacrjournals.org/cancerres/article-pdf/doi/10.1158/0008-5472.CAN-22-0325/3186457/can-22-0325.pdf by University College of London user on 08 August 2022

Figure 1

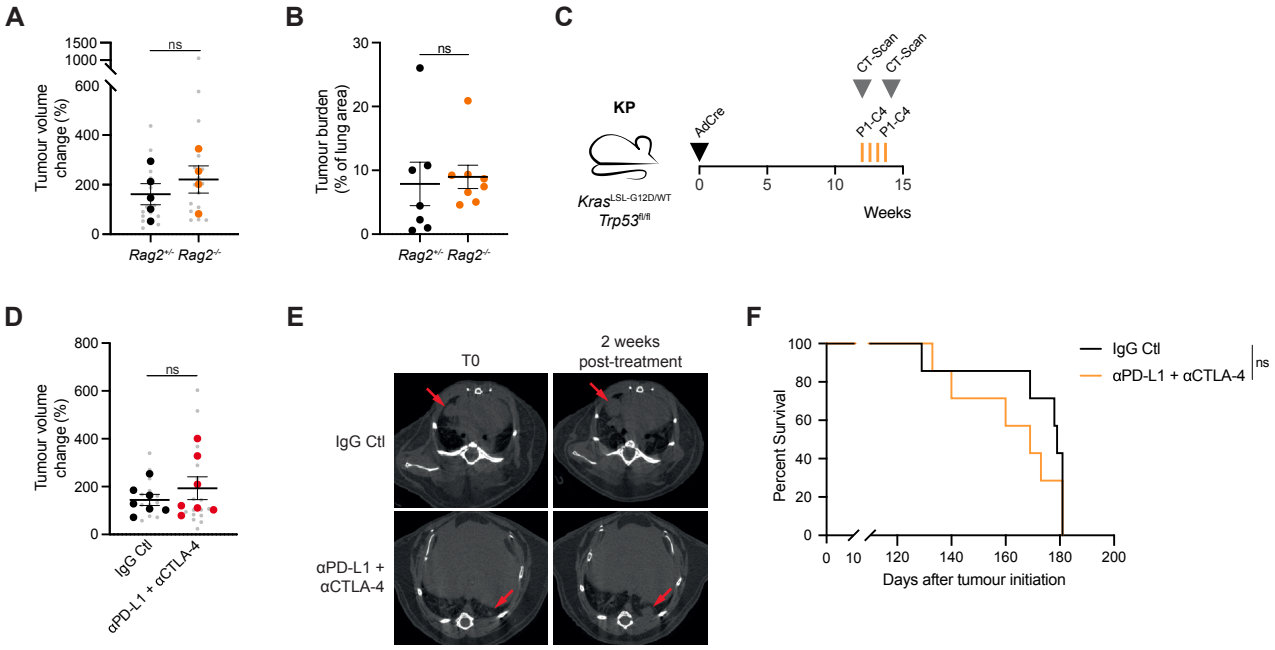

Downloaded from http://aacrjournals.org/cancerres/article-pdf/doi/10.1158/0008-5472.CAN-22-0325/3186457/can-22-0325.pdf by University College of London user on 08 August 2022

Figure 2

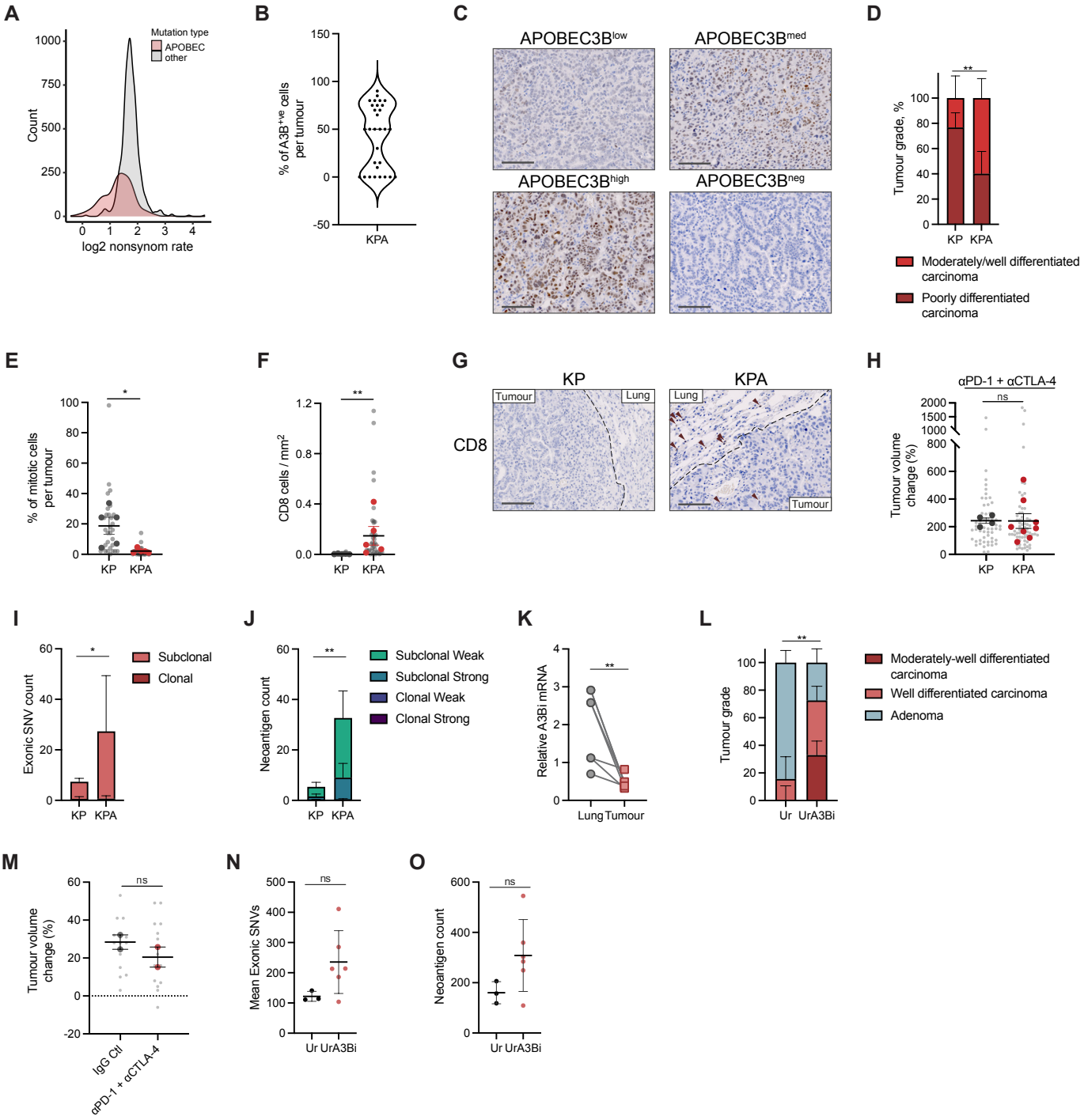

Downloaded from http://aacrjournals.org/cancerres/article-pdf/doi/10.1158/0008-5472.CAN-22-0325/3186457/can-22-0325.pdf by University College of London user on 08 August 2022

Figure 3

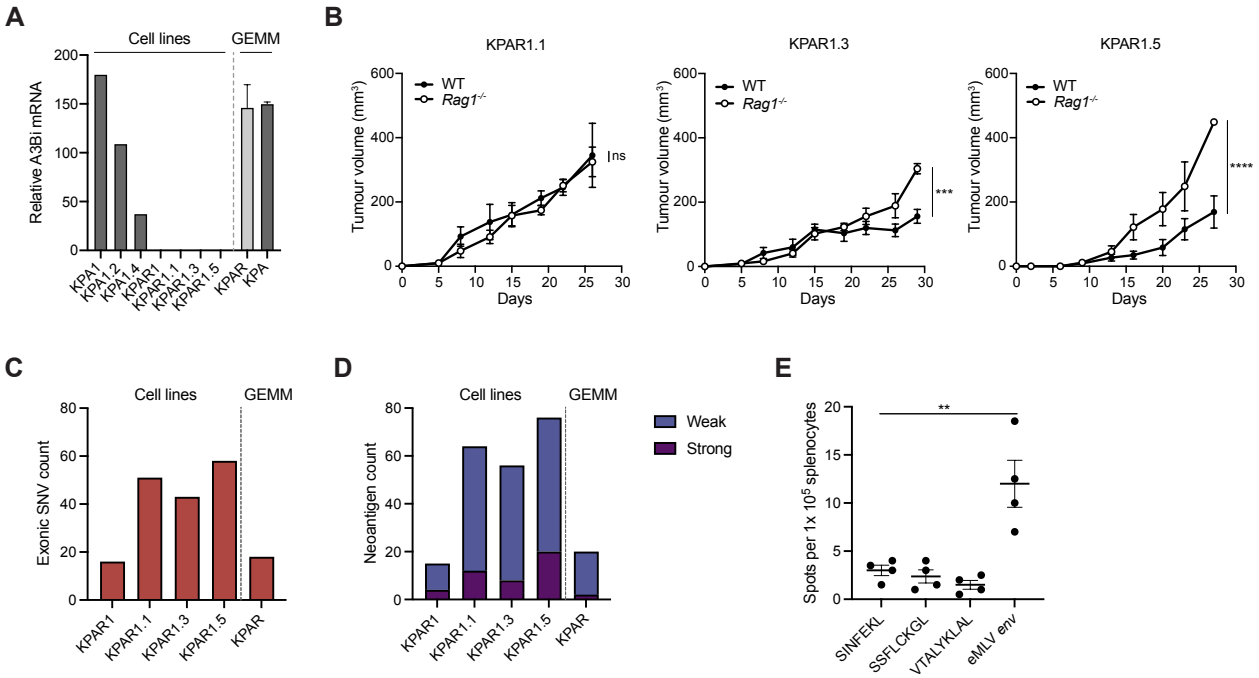

Downloaded from http://aacrjournals.org/cancerres/article-pdf/doi/10.1158/0008-5472.CAN-22-0325/3186457/can-22-0325.pdf by University College of London user on 08 August 2022

Figure 4

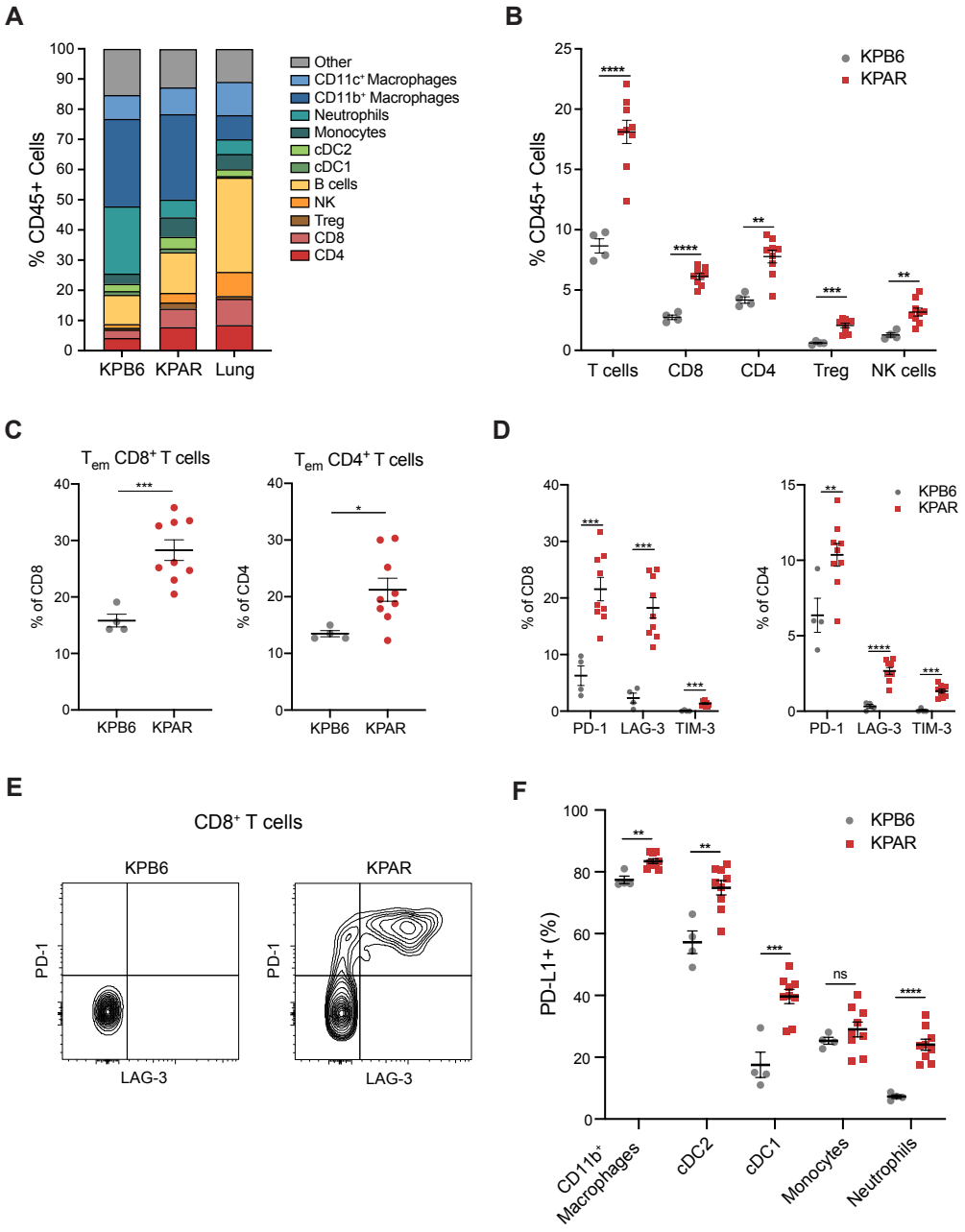

Downloaded from http://aacrjournals.org/cancerres/article-pdf/doi/10.1158/0008-5472.CAN-22-0325/3186457/can-22-0325.pdf by University College of London user on 08 August 2022

Figure 5

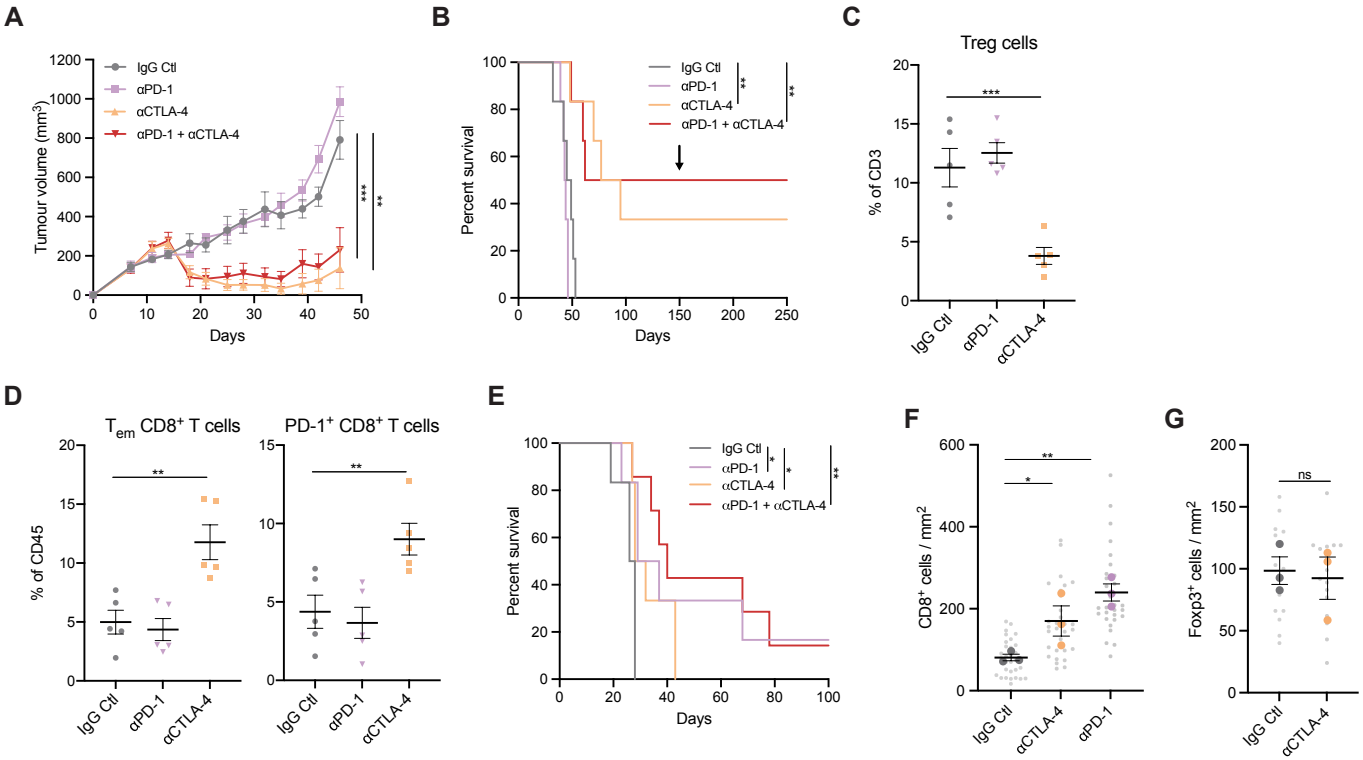

Downloaded from http://aacrjournals.org/cancerres/article-pdf/doi/10.1158/0008-5472.CAN-22-0325/3186457/can-22-0325.pdf by University College of London user on 08 August 2022

Figure 6

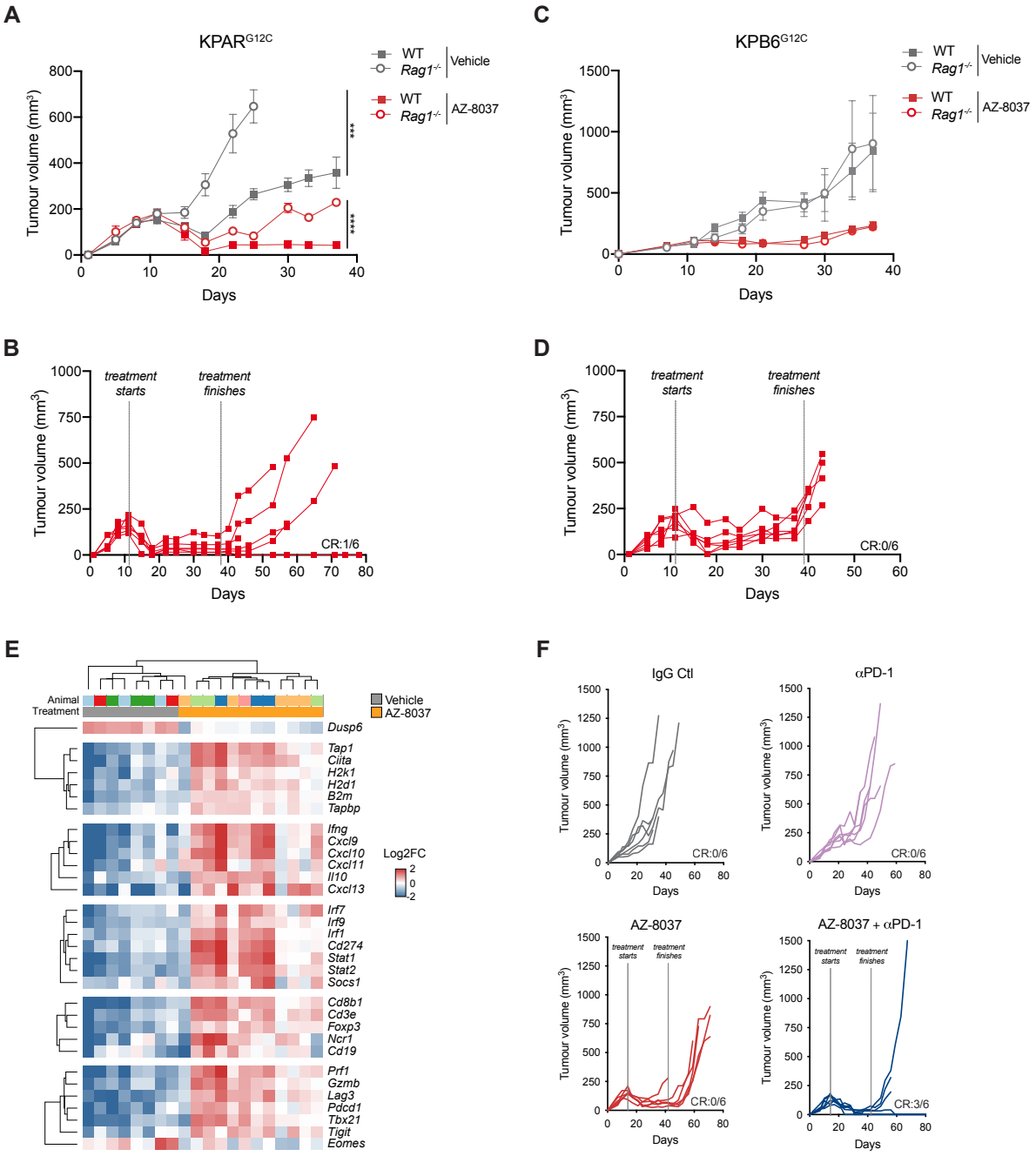

Downloaded from http://aacrjournals.org/cancerres/article-pdf/doi/10.1158/0008-5472.CAN-22-0325/3186457/can-22-0325.pdf by University College of London user on 08 August 2022